Soil Dynamics and Earthquake Engineering 103 (2017) 1–14

Contents lists available at ScienceDirect

Soil Dynamics and Earthquake Engineering

journal homepage: www.elsevier.com/locate/soildyn

A centrifuge-based experimental verification of Soil-Structure Interaction effects

Panagiotis Martakis[a], Damoun Taeseri[a], Eleni Chatzi[a,*], Jan Laue[b]

[a] Department of Civil, Environmental and Geomatic Engineering, ETH Zurich, Switzerland
[b] Department of Civil, Environmental and Natural Resources Engineering, Luleå University of Technology, Sweden

ARTICLE INFO

Keywords:
Soil Structure Interaction
Centrifuge modeling
Experimental verification
Impulse response
SDOF systems
Modal identification
Energy dissipation

ABSTRACT

A series of prototype dynamic centrifuge experiments is carried out to investigate the influence of soil properties and structural parameters on the Soil Structure Interaction (SSI) effect. Established analytical models are herein experimentally verified, and are proven accurate in estimating the system's natural frequency characteristics. It is observed that period elongation is strongly correlated to the relative superstructure-foundation stiffness. Although the present study deals exclusively with the small-strain near-linear range, the experimental response indicates occurrence of nonlinearity. The identified damping results remarkably larger than its analytical estimate and proves highly strain-dependent, raising questions on the reliability of existing analytical methods in capturing the actual dissipation mechanisms. An extended experimental dataset is formed under realistic stress and strain soil conditions, and is implemented, for the first time, for verification of existing analytical models offering valuable insight into the theory and serving as a benchmark for engineering practice.

1. Introduction

The interaction between the superstructure, the foundation and the subjacent soil has been proven to substantially influence the dynamic response of structures and is usually referred to as Soil Structure Interaction (*SSI*), or Soil Foundation Structure Interaction (*SFSI*). This phenomenon is relevant across a range of disciplines, ranging from geotechnical and earthquake engineering all the way to marine and offshore structures. The deformability of the supporting soil affects the global dynamic response by introducing translational and rotational degrees of freedom to the system foundation, thereby resulting in increase of the fundamental period of the overall system, as well as energy dissipation through wave radiation and hysteretic behavior of the soil [1]. SSI effects can be categorized into inertial interaction effects, kinematic interaction effects and soil-foundation flexibility effects [2].

The SSI phenomenon has been a point of academic interest in soil dynamics and earthquake engineering for more than forty years. From the inceptive work of Veletsos and Verbic [3] and the analytical formulations of Gazetas [4,5], to the recent experimental and analytical works of Anastasopoulos [6–8] the understanding of the complexity of this phenomenon continues to evolve. SSI effects have traditionally been considered as beneficial to the dynamic response of structures. In this context, their omission is assumed to lie on the safe side and, thus, many seismic design codes (ATC-3, NEHRP-97) suggest their omission. In design practice SSI effects are only considered for highly sensitive structures founded on sensitive ground. According to Mylonakis and Gazetas [9] this tendency reflects the simplifying assumptions adopted by the actual design provisions for the estimation of seismic demand.

According to the same authors however, existence of seismic records of larger spectral values at the longer period-range indicates the possibility for increased seismic demand owing to the SSI effect. Furthermore, in the case of stiff structures, the period elongation effect results in higher seismic demand. Period lengthening further increases displacement demand and consequently the structural ductility demand. This can be critical for slender structures in terms of serviceability and second order effects. Lastly, the period shift due to SSI could lead to resonance effects with detrimental implications, when the fundamental frequency of the soil-structure system approaches the frequency peak of the excitation, or the eigenfrequency of the soil. In all aforementioned cases, negligence of SSI effects is not to the side of safety.

The present work aims to shed light on the understanding of the SSI phenomenon through a parametric experimental study conducted in a centrifuge facility. The main focus is put on the linear, or rather near-linear, range of the response in order to study the influence of various soil and structural parameters on the modal characteristics of the

Abbreviations: FS_v, Foundation Safety Factor against vertical loads; PLR, Period Lengthening Ratio; SDR, System Damping Ratio; IDR, Identified Damping Ratio

* Corresponding author at: Department of Civil, Environmental and Geomatic Engineering, ETH Zurich, Switzerland.
E-mail address: chatzi@ibk.baug.ethz.ch (E. Chatzi).

http://dx.doi.org/10.1016/j.soildyn.2017.09.005
Received 24 April 2017; Received in revised form 19 August 2017; Accepted 11 September 2017
Available online 24 September 2017

Nomenclature

Geometric parameters

B	width of a rectangular footing or diameter of a cylindrical footing
D	depth of embedment
h	height of the column
H	effective height of the equivalent SDOF model

Material properties parameters

G_o	shear modulus of soil
v	Poisson's ratio of soil
ρ	density of soil

Foundation impedance parameters

K_c	static stiffness of the SDOF model, assuming fixed base conditions
K	static stiffness referred to the foundation base
C	radiation dashpot coefficient

Dynamic properties parameters

M	concentrated mass of the superstructure
f_c	eigenfrequency of the superstructure, assuming fixed base conditions
ω	circular frequency of the response
f	frequency of the response
f_D	damped frequency of the response
$\zeta_{radiation}$	radiation damping ratio of the soil
ζ_c	structural damping ratio
ζ_{mat}	material damping ratio, referred to the hysteretic action of the soil

Dissipated energy method parameters

u(t)	displacement response history of the equivalent SDOF system
v(t)	velocity response history of the equivalent SDOF system
$E_{kin}(t)$	kinetic Energy response history of the equivalent SDOF system
$E_{pot}(t)$	potential Energy response history of the equivalent SDOF system
$E_{tot}(t)$	total Energy response history of the equivalent SDOF system
E_D	dissipated Energy in one vibration cycle
ζ	estimated damping ratio of the system, based on the dissipated energy method

Subscripts

h	horizontal
r	rocking
sys	system soil, foundation and superstructure

structure-foundation-soil system. For the first time, a large amount of dynamic experiments consistently simulating realistic stress and strain soil conditions is carried out to verify established analytical models for prediction of soil stiffness and damping [4,5]. These formulations have so far been validated either numerically or experimentally through statically imposed loads, albeit failing to capture the dynamic characteristics of the SSI system [10]. A previously reported experimental study of small scale dynamic experiments has been limited to the1g gravitational level, failing to realistically simulate the stress and strain conditions of the soil [11,12]. A first preliminary insight to the problem treated herein was offered in [13]. In what follows, the state-of-the-art is broken down into the major thematic areas tied to this investigation, in an attempt to offer a comprehensive overview for the interested reader.

2. Fundamental concepts

In this section we describe the main benefits of centrifuge experimentation, as well as an overview of fundamental energy dissipation mechanisms that comprise the basis for the identification of the system damping.

2.1. Centrifuge modeling

The impedance of the soil is inextricably connected to the existing stress conditions. Thus, reproducing the large confining stresses that are observed even at relatively shallow foundation depths is crucial for the realistic modeling of soil-structure systems. As mentioned in [14], this stress-dependency is a key challenge in laboratory geotechnical modeling. The scaling of structural systems has long been studied and generally proven to provide meaningful results. A thorough work on the scaling of structural models under dynamic loading can be found in [15–17]. For geotechnical applications though, scaling of the stress distribution in the subsoil is non-trivial, while the behavior under the lower stress level of the scaled soil-profile cannot be reliably related to the prototype model. In this respect, centrifuge testing, which allows for one-to-one scaling of stress and strain distribution, becomes a powerful tool for geotechnical experiments. The adopted scaling laws for centrifuge experiments are described in [15–17], while scale effects associated to the underlying assumptions are outlined in [15,18]. These effects are found to bear negligible influence in the design of the present experiments.

2.2. Energy dissipation mechanisms

Despite the extensive research in the topic of soil dynamics, understanding of damping mechanisms remains primitive. Nevertheless, three main mechanisms of energy dissipation in SSI systems are broadly accepted. Firstly, radiation damping, which is highly frequency dependent, increases with the foundation width and embedment depth and is higher in case of deep homogeneous soil deposits [19]. Secondly, material or hysteretic damping, which is usually simulated as equivalent viscous damping, albeit unrealistic since the experimental experience indicates a strain-dependent hysteretic damping, especially for larger strains [20]. To incorporate hysteretic material damping and preserve causality, nonlinear frictional elements were derived by Meek and Wolf [21]. Finally, structural damping is usually modeled as equivalent viscous damping and assumed to be constant for each mode of vibration.

3. State-of-the-art in experimental SSI investigation

The significance of experimentation is ubiquitously recognized throughout engineering fields. Particularly in the domain of SSI, where numerous analytical and numerical models have been developed, experimental verification is necessary for proving these model reliable and actionable. According to [22], experimental studies on the dynamic response of foundation can be grouped in the three following categories:

1. Measurements of the response of actual foundations subjected to dynamic loading (**case-histories**).
2. Small- or large-scale **field experiments** under controlled conditions, in selected sites.
3. Small- and very small-scale **laboratory experiments**, usually conducted on soil placed in a strongbox, with the footing undergoing steady-state or transient vibrations. Experiments in centrifuge constitute a special case of this category.

Despite limited data, case-histories constitute the most generally accepted reference point for engineering research, since they reflect actual conditions alleviating scaling assumptions. A very interesting study in this domain is described in [23], where the modal and structural parameters of four real seismic isolated bridges are identified from acceleration response data throughout 18 earthquakes. Most relevant, within the framework of SSI research, is the observation on the SSI effects resulting more pronounced in cases of softer soil properties, where, most importantly, an even stronger linear relation between the SSI effect and the relative stiffness of the superstructure and the foundation is identified. It is further noticed that the equivalent shear modulus of the soil is significantly reduced during "moderate earthquakes", which should be taken into account for the computation of the foundation impedance.

Another case study is reported in [24], based on the recorded acceleration response of a three-span curved highway bridge under actual ground motion excitations. The authors underline the dependency of the modal characteristics on earthquake intensity, noting extended period lengthening effects, as well as increased damping with increasing earthquake intensity. The period lengthening is attributed to the softening of the soil surrounding the foundations during shaking, rather than structural damage, since the latter is not observed during visual inspection of the bridge. Finally, the authors highlight the reliability of the implemented identification methods in capturing the eigenfrequency of the system, and the unsuccessful identification of the damping ratio, which is estimated with a large relative error of 150%.

A comprehensive overview of measurements conducted on an actual bridge pier, along with laboratory-scaled experiments and numerical simulations is offered in [25], where the importance of the reliable estimation of soil properties for extended bridges under ambient and low-amplitude vibrations is highlighted. A series of field experiments studying the dynamic behavior of a large-scale concrete bridge-pier founded on realistic soil conditions, is presented in [26,27]. The measured response was utilized to verify analytical, as well as numerical models. Effort is put in linking structural damage to variations in the dynamic response. Analytical expressions of the soil compliance are verified in the elastic range. Moreover, the measured nonlinear response of the bridge-piers reveals an increase in the system damping ratio, which is attributed to concrete cracking observed on the pier, as well as to the SSI effect.

The vast majority of small scale experiments in the field of SSI focus on the highly nonlinear range of the response, which is observed for large soil strains mobilized during intense ground motion excitations. The most pronounced effect is the increase of energy dissipation through the hysteresis. An extensive centrifugal experimental study on the nonlinear load-deformation behavior of shear wall footings during cyclic and seismic loading is published in [28]. It is evident that the hysteretic action of soil offers remarkable potential for energy dissipation during dynamic loading. Another important observation is the progressive softening of the soil due to increasing rotation, which is attributed to "uplift and separation of the footing from the soil". The limited confidence to be allocated in soil properties, as well as the large permanent deformations have so far prevented consideration of the hysteretic energy dissipation mechanism for reducing the ductility demand on the superstructure. In this direction, a new seismic design philosophy that considers the SSI as a design parameter by redirecting failure to the soil has already been proposed in [6], termed as "rocking isolation". However, the above-mentioned issues have to be thoroughly taken into account by the designer. Subsequent works [29,30] investigate the effectiveness of soil improvement to reduce the accumulated settlements by increasing the static safety factor for bearing capacity (FS_v). It is concluded that soil improvement "may be quite effective provided that its depth is equal to the width of the foundation" [29]. It is further mentioned that in case of large safety factors ("larger than 10 for sand"), the foundation responds through uplifting, while in case of lower safety factor ("up to 5 for sand"), the response is "sinking dominated", due to accumulated settlements. The uplifting response is preferable, since it does not yield permanent settlements.

The near-linear range of the response has so far been experimentally studied through static imposed loading, failing to capture the dynamic characteristics of the SSI system. A single experimental study exists on small-scale dynamic experiments focusing on the near-linear range of the response [11,12], which overviews 54 free-vibration 1 g tests of small scale footing-models embedded in sand. This parametric experimental campaign investigates the influence of the foundation shape (circular, square and rectangular) and embedment depth on the dynamic response of footings founded in a, reasonably assumed as, homogeneous half-space. Free vibration is triggered by the sudden release of suitable static loads that independently excite each mode: vertical, torsional and swaying-rocking mode. The response is recorded with velocity transducers located at the top of a block. All damping ratios were calculated using the logarithmic decrement method. The identified frequencies and damping ratios were analyzed in subsequent works [22,31], in order to verify the homogenous half-space analytical solutions proposed in [4]. It should be noted that the shear-wave velocity introduced to the analytical model is back-calculated from the measured swaying-rocking natural frequencies of the surface footings. Finally, the theoretical estimation of damping refers to radiation damping, while a constant value of 2.5% was adopted for the material

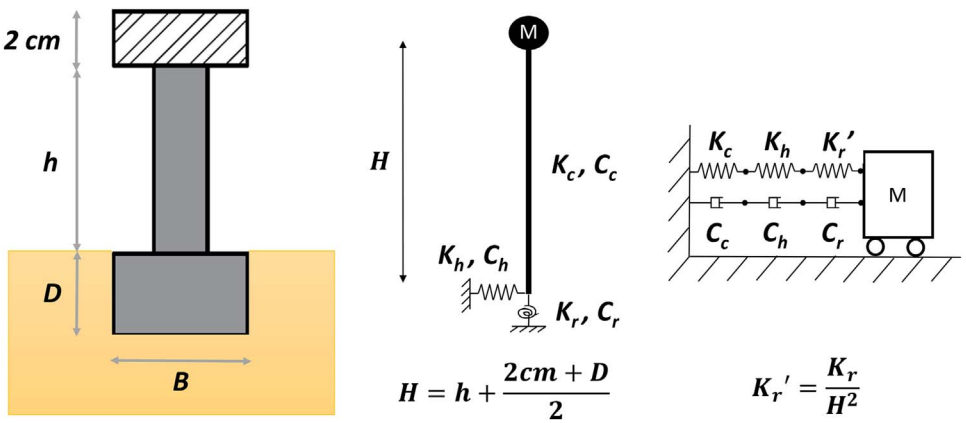

Fig. 1. Left: planar sketch of a typical model geometry, middle: lumped mass SDOF model, right: equivalent simplified SDOF model.

damping. For all modes, theoretical predictions, and experimental measurements of natural frequencies agree within a 10% margin, provided that an effective soil shear modulus is judiciously chosen for each vibration mode. It should be mentioned however, that small-scale experiments conducted in gravitational level of 1 g do not allow for one-to-one scaling of stress and strain distribution. The soil behavior under the lower stress level of the scaled soil-profile cannot be reliably related to the prototype model, since the impedance of the soil is inextricably connected to the existing stress conditions. Thus, reproducing the large confining stresses that are observed even at relatively shallow foundation depths is crucial for the realistic modeling of soil-structure systems. As mentioned in [14], this stress-dependency is a key challenge in laboratory geotechnical modeling, successfully tackled via centrifuge experiments.

The present work aims to study the influence of various soil and structural parameters on the modal characteristics of the structure-foundation-soil system through a parametric experimental study conducted in a centrifuge facility. For the first time a broad dataset of dynamic experimental data is generated to consistently approximate realistic stress and strain soil conditions, in order to verify established analytical models for estimation of the system's modal characteristics [4,5]. The following chapter presents the analytical formulation on the modal characteristics of the modeled SSI system, along with necessary assumptions. Metrics for quantification of the SSI effect are also explained. Chapter 5 overviews the experimental setup as well as the test procedure.

4. Analytical SSI formulations

4.1. Analytical model

A simplified lumped mass SDOF model is selected for the analytical formulation of the problem addressed herein (Fig. 1 middle). Since the impulse load is applied on the top of the structure, the first coupled rocking-swaying mode is primarily excited and therefore no additional degrees of freedom are herein introduced. A comparison to the predictions of analytical models considering more degrees of freedom confirms this statement, in that the resulting modal characteristics of the first mode demonstrate negligible deviations from the SDOF model prediction. The following assumptions are adopted for transitioning from the 3D physical model to the simplified lumped-mass SDOF model presented in Fig. 1 (middle):

- Since the structure is excited in one direction, this is simplified into a planar problem (Fig. 1 left). The interested reader is nonetheless pointed to [32] for a 3D study of the rocking phenomenon.
- The mass is assumed as lumped on the top of the structure. The half-mass of the column is added to this mass.
- The aluminum footing is assumed to be rigid and massless.
- The midpoint of the foundation is considered as the center of rotation for the rocking spring.
- The axial and shear stiffness of the columns are assumed infinite.
- In the vertical direction the soil is considered to be incompressible; an assumption confirmed by large static safety factors against vertical loads ($FS_V > 10$) [33].
- Since the intensity of excitation remains low, the equilibrium is calculated according to the first order theory.

The stiffness and the damping of the system are modeled via springs and dashpots respectively, according to the methodology described in [4]. The structural damping ratio of the aluminum models is measured experimentally [33] and the average value of 1.5% is adopted for the analytical model. The dynamic impedance of the soil is calculated for the swaying-horizontal mode (h) as well as for the rocking (r) response, according to the aforementioned methodology [4], by introducing the foundation geometry, soil properties (G_o, ρ, ν) and the damped oscillating frequency of each mode into the formulation. Since the oscillating frequency is an input parameter in this context, an iterative process is necessary for the estimation of dynamic impedance.

With all the stiffness and dashpot coefficients computed, the effective stiffness of the SDOF model may be estimated as a serial arrangement of the springs and the dashpots (Fig. 1 right).

$$\frac{1}{K_h}+\frac{1}{K_r'}+\frac{1}{K_c}=\frac{1}{K_{sys}} \Rightarrow K_{sys}=\frac{K_h\cdot K_r'\cdot K_c}{K_h\cdot K_r'+K_r'\cdot K_c+K_h\cdot K_c} \quad (1)$$

The corresponding equivalent natural frequency of the SDOF system and the fixed-base frequency can be computed as follows:

$$f_{sys}=\frac{1}{2\cdot\pi}\sqrt{\frac{K_{sys}}{M}} \quad f_c=\frac{1}{2\cdot\pi}\sqrt{\frac{K_c}{M}} \quad (2)$$

Two additional system frequencies can be defined: the rigid-body system frequency (a) due to foundation swaying, and (b) due to foundation rocking [34]:

$$f_h=\frac{1}{2\cdot\pi}\sqrt{\frac{K_h}{M}} \quad f_r=\frac{1}{2\cdot\pi}\sqrt{\frac{K_r'}{M}} \quad (3)$$

The corresponding damped frequencies be derived for each mode (j), by assuming viscous damping behavior, as follows [35]:

$$f_{D,j}=f_j\cdot\sqrt{1-\zeta_j^2} \quad (4)$$

The radiation-damping ratios due to the swaying and rocking mode can be evaluated as a percentage of the critical value:

$$\zeta_{h,radiation}=\frac{C_h}{2\cdot M\cdot\omega_h} \quad \zeta_{r,radiation}=\frac{C_r}{2\cdot M\cdot\omega_r} \quad (5)$$

4.2. SSI indices and metrics

4.2.1. Period Lengthening Ratio (PLR)

The fraction of the system-eigenperiod over the fundamental period of the fix-based structure. Period lengthening is a direct result of the existence of deformable soil underneath and surrounding the foundation and therefore constitutes the most common index to quantify the degree of the inertial SSI effects.

$$PLR=\frac{T_{system}}{T_c}=\frac{f_c}{f_{sys}} \quad (6)$$

4.2.2. Soil Structure Interaction index (SSI_{index})

The ratio of the physical flexural stiffness of a bridge pier (assuming rigid foundation) over the identified stiffness of the bridge pier-foundation-soil system [23]. This index practically contains the same information with the PLR, which in this case does not depend on the mass. Consequently, it can be used to compare the degree of inertial SSI effects between models with different masses.

$$SSI_{index}=\frac{K_c}{K_{sys}} \quad (7)$$

4.2.3. System Damping Ratio (SDR)

The System Damping Ratio refers to the contribution of the foundation damping to the system damping and expresses the combined effect of all damping mechanisms acting in the system. An approximate expression, weighting the contribution of each damping mechanism depending on the fundamental frequency of the system, is suggested in [10]. It should be noted that the material damping is considered as a constant value, in compliance with the suggestions of [4].

$$SDR = \left(\frac{f_{sys}}{f_h}\right)^3 \zeta_{h,radiation} + \left(\frac{f_{sys}}{f_r}\right)^3 \zeta_{r,radiation} + \left(\frac{f_{sys}}{f_c}\right)^3 \zeta_c + \left(1 - \left(\frac{f_{sys}}{f_c}\right)^2\right) \zeta_{mat} \quad (8)$$

5. Experimental procedure

5.1. Laboratory setup

The experiments were performed in the drum centrifuge facility of the Institute of Geotechnical Engineering at ETH Zurich. The geotechnical drum centrifuge facility is described in detail in [36]. The external radius of the channel is 1.1 m, the height is 0.7 m and the depth is equal to 0.3 m. Models can be tested in strongboxes fixed to the channel of the drum. For the purposes of these experiments, a pair of cylindrical strongboxes are utilized. The internal dimensions of the boxes are 400 mm (diameter) and 200 mm (height), corresponding to 40 m and 20 m respectively in a 100 g test. An outline of the test layout is given in Fig. 2.

In order to generate an impulse-type excitation, a prototype tube-mechanism was developed, so as to shoot -in flight- small drop weights (spheres) against the top of the structure. The lower part of the tube is attached to an actuator-arm and rotates together with the drum channel and the tool platform, targeting the head of the structure, as shown in Fig. 4. The upper part leads to the top of the safety shield to a rotary coupling, which allows spheres to be dropped from the stationary into the rotary environment. The rotating part of the pipe accelerates the spheres before they hit the structure. Different kinds of spheres, in terms of material, radius and weight, were used to achieve different levels of intensity. The properties of the spheres are described in Table 1.

The instrumentation comprises four miniature uniaxial accelerometers, manufactured by Bruel und Kjaer, which provide an almost flat (± 5%) frequency response in the range of 1–10,000 Hz. They are positioned as follows: (1) vertically on the top of the foundation, (2) horizontally, parallel to the direction of the excitation, on the top of the foundation, (3) horizontally, parallel to the direction of the excitation and (4) horizontally, perpendicular to the direction of the excitation, on the top of the mass (Fig. 3).

5.2. Model preparation

The soil material used is Perth-Sand with a maximum diameter of 0.2 mm; with mechanical properties as described in [37]. One of the critical parameters investigated in these experiments is the influence of the soil stiffness on the SSI effect, which is analytically considered through an average value of the secant shear modulus of the soil at the gravitational center of the foundation. The shear-modulus highly depends on the density of the sand layer, which can be defined during the preparation of the soil-model. The preparation of the model should also ensure that models are built under similar conditions in order to guarantee the repeatability of the tests. A broadly used method for the soil preparation that conforms to the above requirements is dry-pluviation. The depositional intensity, defined as the weight of soil falling per unit area per unit time [38], as well as the height from which the sand falls, are highly correlated to the dry density of the sample [37]. In general, larger densities are obtained with higher falling height and smaller depositional intensity, although the trends are not fully uniform [37]. In the framework of these experiments the falling height was kept constant, equal to 40 cm for all the models. The different depositional intensities (volume flow) achieved vary between 1 and 167 g/min/cm^2. The samples prepared with depositional intensities between 1 and 8 g/min/cm^2 comprise an average dry density of 1,72 t/m^3 and are regarded as “dense”. Samples of depositional intensities between 112 and 167 g/min/cm^2 results in an average dry density of 1,67 t/m^3, and would be considered as medium-dense but are labeled as “loose” in this context for comparison reasons. Although the different order of depositional intensities does not yield a remarkable difference in terms of dry density, however, it proved to be large enough to affect the system response.

The model represents a SDOF system embedded in homogenous sand. The dimensions have to comply with the restrictions of the centrifuge strongbox, while the dynamic characteristics should be representative of real structures. Last but not least, the model should be easy to build and the model-costs should be minimized, since a series of experiments was to be conducted. In this framework, fourteen (14) models with square foundation and different geometries were designed and constructed in the workshop of the department of civil engineering at ETH. The dimensions of these models are summarized in Table 2. All models feature the same steel mass on the top, while the column height, the foundation depth and the foundation width vary. Another fourteen (14) models were constructed featuring circular foundation, while maintaining all other dimensions unchanged (the column shape remains cylindrical and the foundation width is equal to the diameter of the corresponding square footings). For labeling reasons, the models are named after the serial number assigned in Table 2, followed by ‘s’ for square foundation or ‘c’ for circular foundation. For the initial design of these models, a rough estimation of the average value of G-modulus in the topmost 2 m of the soil was assumed to be equal to 50 MPa. By adopting this value at the gravitational center of the foundation, the analytical models, described in the analytical part, provide an estimation of the eigenfrequency of the system. A total of 58 experiments were successfully conducted, providing an adequate amount of information for the subsequent analysis (Table 3). The procedure followed for the preparation of the centrifuge models is described in detail in [33].

5.3. Test description

Each experiment comprises three stages, when the acceleration response of the system due to excitations of different impulses is measured. The experiment initiates with the increase of the centrifugal acceleration from 0 to 60 g. The lower edge of the shooting tube is attached to an actuator, which rotates together with the drum channel and may move locally, independently from the rotation of the centrifuge. The movement of the actuator is operated -on flight-: the lower edge of the shooting tube is placed adjacent to the head of the structure, with an angle of 45°, so as to ensure that the sphere will be reflected to the soil after the hit. At this position, the lower edge of the shooting tube targets the middle of the structure head, as shown in Fig. 4. At this point, the first session of measurements is recorded. At 60 g, only the lighter spheres with labels 1a to 3 are shot, in order to avoid plastic deformations. The initial experiments indicated that heavier metallic spheres (with labels: 4–7) cause a highly nonlinear response, which is out of the focus of the present thesis and thus, neglected. Subsequently, the centrifugal acceleration increases to 100 g. The system then corresponds to a different prototype equivalent. This time the structure is

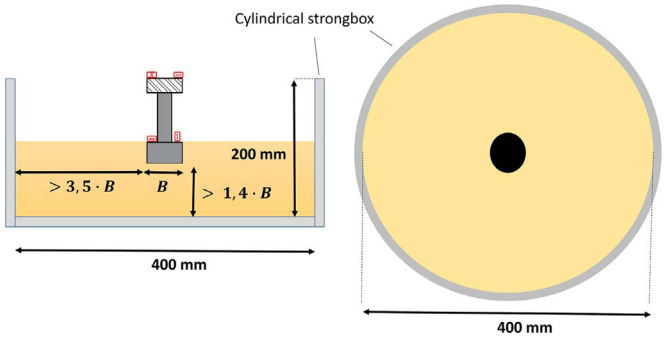

Fig. 2. Centrifuge test layout: left: cross-section, right: ground plan.

Table 1
Characteristics of the spheres used for the impulse excitation.

Ball Id	1a	1b	1c	2	3	4	5	6	7
Material	*Plastic*	*Plastic*	*Plastic*	*Plastic*	*Plastic*	*Steel*	*Steel*	*Alum*	*Steel*
Mass[g]	*0.08*	*0.15*	*0.33*	*0.51*	*0.70*	*0.88*	*1.40*	*1.65*	*4.08*

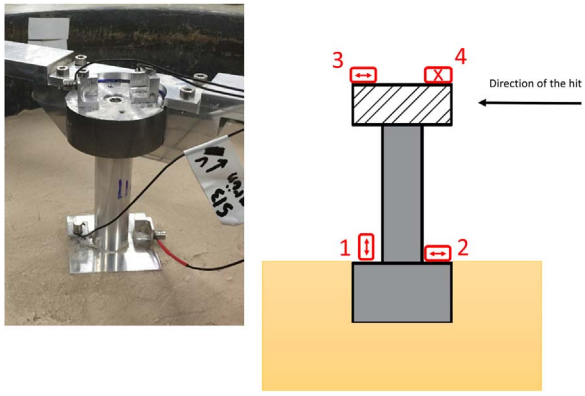

Fig. 3. Left: picture of the instrumentation, right: schematic representation of the experimental instrumentation. The arrows indicate the direction of the accelerometers.

shot with all available spheres (labels 1a to 7). Next, the structure is once again shot with spheres 1a to 3, so as to compare the difference of the 'elastic' response prior to and after the shooting of heavier spheres. After the last shot, the centrifuge is stopped.

6. System identification across scales

The system response is studied on the basis of the output-only acceleration data recorded on the top of the structure, parallel to the motion (accelerometer 3 in Fig. 3). The sampling rate of the data acquisition system was set to 60 kHz. The analytically derived frequencies provided an estimation of the frequency range of interest for the first mode, which proved to be in the range of 150–350 Hz for the scaled models, which corresponds to 1,5–6 Hz for the equivalent prototype system. The signals were then down-sampled to 10 kHz for the further processing. In the following, all information will be expressed at the scale of the equivalent prototype system.

6.1. Frequency identification

A typical response spectrum of the equivalent prototype system is presented in Fig. 5 (upper right). The damped natural frequencies of the system are directly identifiable from the spectrum. The lowest eigenfrequency renders a clear spectral peak, since the resulting deformed shape concurs with the first coupled rocking-swaying mode of the system. Since the first rocking mode is primarily activated, the subsequent analysis deals exclusively with this mode. To this end, a low-pass Butterworth filter with a Nyquist frequency of 5 Hz is applied, in order to reduce the noise and focus on the frequency range of interest (1,5–6 Hz).

A comparison between the original and the filtered signal is offered in Fig. 5 (upper left). The transient, high-frequency response that is observed at the beginning of the oscillation corresponds to higher modes of the model that are not examined in the framework of this work and thus they are filtered out. In order to track the evolution of the spectral content of the response, a *spectrogram plot* is offered in Fig. 7 (lower left). The eigenfrequency of the system is reduced by almost 11% before eventually reaching a constant value. This very important observation indicates a nonlinear response during the first cycles of the oscillation.

Table 3
Description of the 58 conducted experiments.

Foundation	*Square*				*Circular*	
Soil	Loose		Dense		Loose	
Gravitation	60 g	100 g	60 g	100 g	60 g	100 g
Tests run	14	11	14	11	4	4

6.2. Moment-rotation behavior

The moment-rotation behavior provides valuable information regarding the stiffness and the energy dissipation of SSI systems, especially when rocking response proves dominant. Several recent studies in the domain of SSI deal with this behavior, mostly under cyclic loading in the nonlinear range, where the hysteretic action of the soil becomes significant [28,29,39]. Before reaching the nonlinear plateau, the response is considered to be linear elastic and the energy is assumed to be dissipated mostly through radiation. Nevertheless, indications of nonlinearities in the small strain-level have already been mentioned in [40]. No experimental studies regarding this phenomenon for SSI systems were found. Hence, the plot of the moment-rotation response for the present free vibration experiments is of particular importance, especially after indications of nonlinear behavior in the first oscillation cycles in terms of frequency-shift.

The methodology followed for the development of moment-rotation plots is based exclusively on the acceleration measurements and is described below:

1) A high-pass Butterworth filter with $f_{Nyquist} = 1$ Hz is applied to the detrended acceleration signal, in order to discard the low-frequency noise. As a result, potential nonlinear effects from displacements in this range are inevitably discarded.
2) The acceleration signal is numerically integrated, yielding the velocity response
3) The same high-pass filter is applied to the velocity signal.
4) The velocity signal is numerically integrated, yielding the displacement response
5) The same high-pass filter is applied to the displacement signal.

Trapezoidal numerical integration is then carried out. A typical acceleration response of the prototype system is shown in Fig. 5 (upper left) for lighter spheres (up to number 3), and in Fig. 5 (lower left) for the heavier spheres (number 4–7). As observed, in the former case the system oscillates harmonically, indicating that the response remains within the "elastic" range. For the heavier spheres, however, the response reaches the inelastic region: permanent deformations appear, indicating dynamic failure of the soil. The unrealistically large value of

Table 2
Dimensions of the models [cm].

Model Id	$1_{s,c}$	$2_{s,c}$	$3_{s,c}$	$4_{s,c}$	$5_{s,c}$	$6_{s,c}$	$7_{s,c}$	$8_{s,c}$	$9_{s,c}$	$10_{s,c}$	$11_{s,c}$	$12_{s,c}$	$13_{s,c}$	$14_{s,c}$
h [cm]	4	5	5	6	6	6	6	6	7	7	7	7	8	8
D [cm]	4	2	3	2	3	2	3	4	2	2	3	4	2	3
B [cm]	4	4	4	4	4	5	5	5	4	5	5	5	5	5

Fig. 4. Left: The shooting tube is attached on the actuator arm, right: the lower edge of the tube targets on the head of the structure with an angle of 45°.

the plastic deformation is a result of the drift in the acceleration signal, which is propagated through the numerical integration.

The present work focuses on the "elastic" (or near-elastic) range and, thus, no further analysis on nonlinear response will be conducted. However, the clear distinction of the response between the lighter and the heavier spheres indicates that response induced via lighter spheres did not approach the nonlinear threshold.

The Moment - Rotation (M-θ) response is calculated directly from the acceleration and displacement time-history by applying the transformations described in Fig. 6. It is noted that the translational mode is neglected, while the structure is assumed as rigid and rotating around the center of mass of the foundation, which corresponds to the first rocking mode. A typical moment-rotation response of the prototype is presented in Fig. 9. The elliptic form of the loops is representative of viscoelastic behavior. The ultimate values of the moment capacity for all the model configurations are calculated according to [41]. For all the examined cases, the moment response remains lower than 10% of the ultimate value.

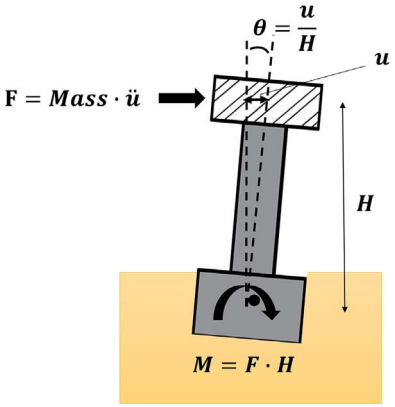

Fig. 6. Moment-rotation estimation.

6.3. Damping identification

As already mentioned, the response amplitudes of the presented experiments remain within the "linear elastic" limits, where the viscous damping assumption is usually adopted. The elliptical shape of the M-θ plots indicates dynamic hysteresis, which may however be approximated via adoption of an equivalent viscous damping. Since free vibration response is studied herein, and the linear range is under investigation, the *logarithmic decrement method* could be adopted. However, the existence of mild nonlinearities yields a curve that may not be fitted via an exponential function and the method would thus not provide reliable estimations. Therefore, a modification of the *Dissipated Energy method* is applied for the estimation of the equivalent viscous damping and proves to give reasonable results.

According to the *Dissipated Energy method*, the damping ratio can be computed by equating the energy dissipation of the actual system with the energy dissipation of an equivalent viscous system during one vibration cycle. This method is mostly applied for cyclic excitation at constant frequency, where steady-state response is reached. In the present case the response is free-vibration and the total amount of input energy is introduced at the beginning through impulse. Afterwards, the response is damped out, without forming closed loops, since the dissipated energy is not compensated. In order to apply the dissipated energy method for free vibration response, some modifications are here considered.

Energy is introduced to the system through impulse on the top of the

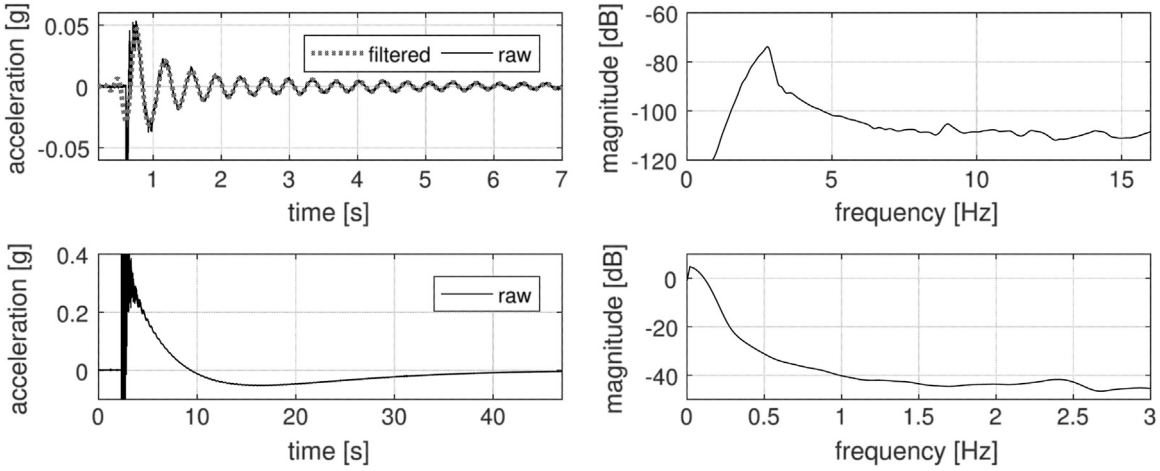

Fig. 5. Typical response of the prototype in time and frequency domain. Upper: for lighter spheres (id: 1a-3), lower: for heavier spheres (id: 4–7).

structure. The exact amount of the input energy may not be computed, although the acceleration response of the system can provide a valuable insight into the energy flow. The velocity and displacement time-histories of the response are obtained through numerical integration. Based on these, the Kinetic and the Potential energy of the system can be computed by introducing the mass and the identified stiffness of the system, while the sum of the kinetic and the potential energy constitutes the total energy of the system.

$$E_{kin} = \frac{1}{2}\cdot M\cdot v^2 \quad E_{pot} = \frac{1}{2}\cdot K_{sys}\cdot u^2 \quad E_{total} = E_{kin}+E_{pot} \tag{9}$$

With the time-history of the total energy defined, the dissipated energy can be estimated as the difference in total energy between two time-points of the response. The dissipated energy in one vibration-cycle is defined as the difference between the initial and the final amount of total energy, at the beginning and at the end of each cycle:

$$E_D = E_{total}(t_1) - E_{total}(t_1 + T_{sys}) \tag{10}$$

The damping ratio can be estimated for each pair of time-points that differ for a time span equal to the period of the system, by introducing the initial total energy and the corresponding dissipated energy of each cycle into the formulation derived for the steady-state case:

$$\zeta = \frac{1}{4\cdot\pi\cdot\omega/\omega_n}\cdot\frac{E_D}{E_{total}(t_1)} \Rightarrow \zeta = \frac{E_{total}(t_1) - E_{total}(t_1 + T_{sys})}{4\cdot\pi\cdot E_{total}(t_1)} \tag{11}$$

The system vibrates freely and thus the excitation frequency is equal to the natural frequency of the system ($\omega = \omega_n$). A characteristic time-history response of the system in terms of acceleration, total energy, damping ratio and eigenfrequency is presented in Fig. 7.

It is remarkable that 90% of the system's energy is dissipated within the first 3 cycles (in other model configurations this ranges extends up to 7 cycles). Interestingly enough, in the same range a “drop” of the eigenfrequency is observed, which indicates nonlinear response. For these reasons, it is reasonable to evaluate the equivalent viscous damping in this range of the response. The method is applied by considering all the peaks of the kinetic and potential energy as reference points, which leads to four estimations of damping pro vibration-cycle. The estimated damping ratios are plotted in time, as shown in Fig. 7, and the average value is estimated. In most cases the damping ratio remains constant and thus the average value can be considered as the equivalent damping ratio of the system.

7. Experimental verification of fundamental theory

As explained in the Analytical Formulation section, an equivalent value of G-modulus has to be assumed for employing the analytical model. The calibrated value of the G-modulus is obtained by minimizing the coefficient of variation (*CV*) between the analytical predictions and the original response. The calibrated values of the G-modulus are summarized in Table 4 for all different soil conditions, where it is evident that the calibrated G-modulus is affected even for slight variations of the dry density of the soil.

Table 4
Calibrated values of the average equivalent G-modulus at the gravitational center of the foundation for the different soil conditions.

	Loose	*Dense*
60 g	31 MPa	36 MPa
100 g	41 MPa	45 MPa

The experimentally obtained eigenfrequencies and the analytical estimations are presented in Fig. 8. In all cases the coefficient of determination results higher than 88% and the *CV* remains lower than 5%. Both indices suggest a very good fit between the simplified analytical model and the experimental results and confirm other experimental studies that reach the same conclusion [22], provided that the equivalent G-modulus of the soil is properly back-calculated.

The damping ratio of the system is identified with a modification of the common *Dissipated Energy method*, which expresses the combined effect of all damping mechanisms acting in the system, modified to apply for free vibration response. From an analytical point of view, the energy dissipation can be assessed by the System Damping Ratio (*SDR*), which has been presented in the Analytical Formulation section. The damping ratio of each dissipation-mechanism is weighted by the ratio of the system-frequency over the corresponding “rigid body” frequency. The radiation damping can be theoretically estimated by applying the methodology described in [4]. The structural and material damping, however, are introduced as constant values and require proper assumptions. Consequently, the radiation damping is the only mechanism that can be analytically modeled, while the structural and the material damping are considered to be constant in the elastic range (lower level of strains). According to [4], for lower levels of strain, the radiation damping constitutes the dominant dissipation mechanism. It is reminded that the response of the system during the experiments theoretically remained in the elastic range, by keeping the Moment response lower than 10% of the ultimate Moment. Thus, it is reasonable to compare the identified damping ratios (*IDR*) with the estimated SDR, by neglecting the material damping in the first place ($\zeta_{mat} = 0$).

The structural damping ratio is experimentally estimated to be equal to 1.5%, while the material damping of the soil is initially

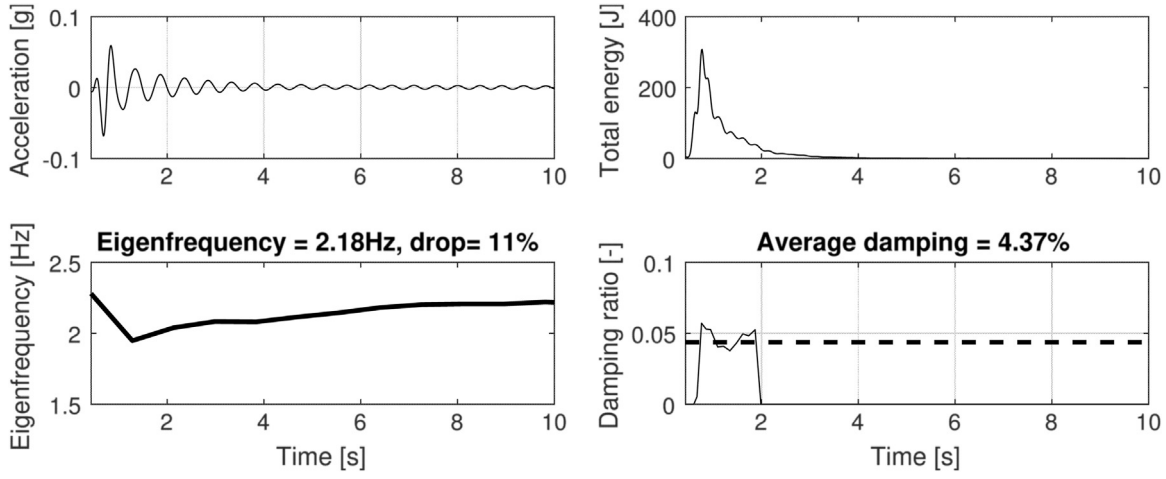

Fig. 7. Typical response of the prototype for lighter spheres. Upper left: acceleration, upper right: total energy, lower left: Eigenfrequency (spectrogram), lower right: identified damping ratio in the part of the response, where the total energy is above 10% of its maximum value.

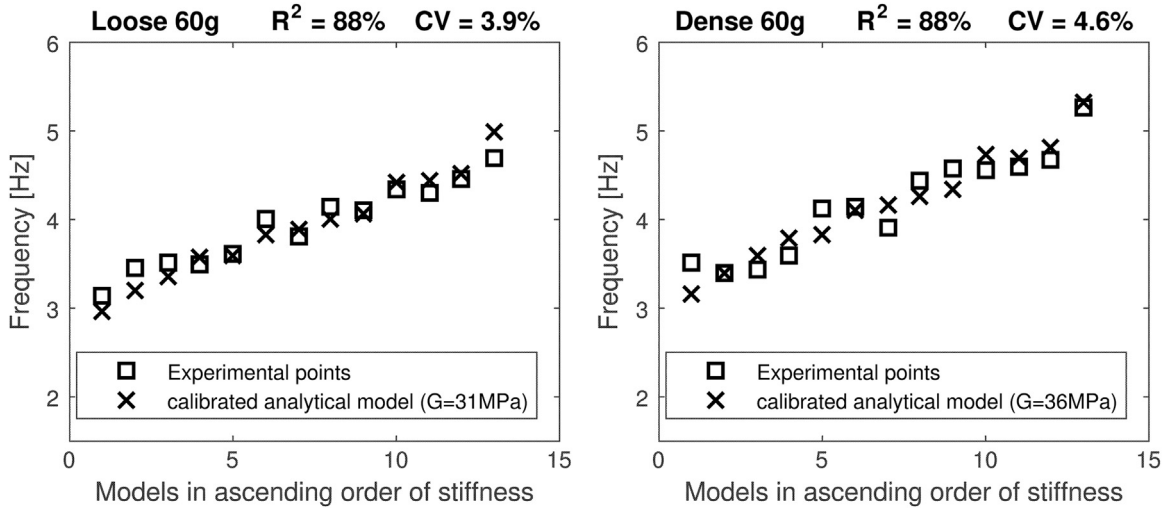

Fig. 8. Analytical fit to the experimentally identified eigenfrequencies.

neglected. It is observed that the weighted contributions of the structural damping and the radiation due to rocking are negligible as well. The analytically computed *SDR* is actually driven by the swaying-radiation damping.

7.1. Parametric study of the dynamic response in the "elastic" range

The dynamic response of the SSI system is studied through the aforementioned SSI indexes. Additionally, the Moment-rotation response provides valuable insights into the stiffness of the system and the energy dissipation. Finally, the eigenfrequency itself constitutes a very familiar expression of the system stiffness in engineering practice and is thus studied independently.

The influence of the following parameters on the characteristics of the response is discussed in the subsequent section:

- The **foundation slenderness**, defined as the ratio of the foundation embedment over the foundation width (*D/B*), as shown in Fig. 1.
- The **relative stiffness** of the superstructure (assuming fixed base) over the foundation stiffness.
- The **impulse intensity**: depending on the size of the spheres that were shot (Table 1)
- The **eigenfrequency** of the free oscillation and the **PLR** are considered as parameters in order to examine the relation between each other and with the other characteristics of the response. A normalized expression for the frequency is implemented, defined as the fraction of the identified eigenfrequency multiplied by the height of the structure over the equivalent shear wave velocity:
- The **soil density**: Two different levels of soil-compaction were achieved (loose/dense).
- The safety factor for bearing capacity (FS_V): the safety factor for each model configuration is calculated according to Terzaghi [42], by considering the effect of embedment [33].
- The **shape of the foundation**: circular and square foundation shapes were tested.
- **Effect of nonlinearities**: as explained, the model is eventually subjected to impulse excitation of larger amplitude that brings the system into the nonlinear range of the response. The system is subsequently subjected to impulses of lower intensity, in order to investigate the possible effect of nonlinearities on the elastic system response.

Increasing the depth of the foundation relative to the width has a direct increasing effect on the system stiffness. The *PLR* does not appear sensitive to this parameter, while the identified damping does not show a clear tendency. The *M-θ* behavior of two extreme cases of foundation-slenderness are presented in Fig. 9. This comparison plot clearly illustrates the effect of the embedment depth on the stiffness of the system.

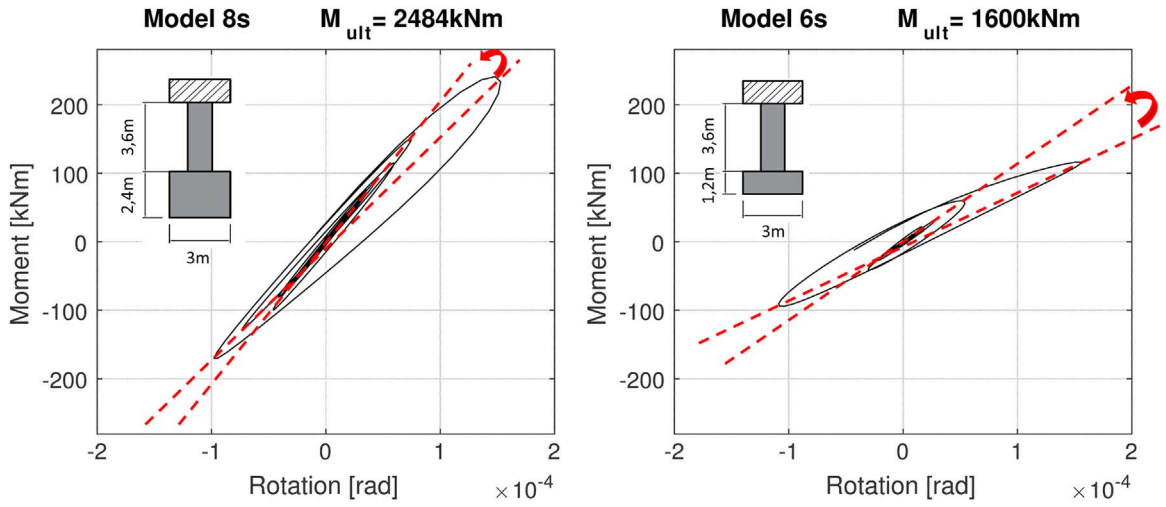

Fig. 9. Moment-rotation response of models with different foundation depth (prototype).

The slope corresponds to the stiffness and increases substantially with increasing embedment. Another interesting observation is that the stiffness appears lower during the first couple of cycles. This "softening" of the system at the beginning of the oscillation, which has already been visualized in the spectrogram plot (Fig. 7), is indicative of nonlinear response. Considering the fact that the Moment-level is lower than 10% of M_{ult}, it is concluded that nonlinear effects are present even in the theoretical "linear elastic" range of the system response, according to elastoplasticity theory.

At this point it should be noted that the rotation of the system is calculated through double integration of the high-pass filtered acceleration signal. As a result, the potential low-frequency nonlinearities of the displacements are inevitably filtered out, and so what is offered is a suboptimal approximation. Utilization of displacement measurements in future tests will be sought to refine this estimation.

The relative stiffness of the superstructure and the foundation indicates a strong relation to the *PLR* and consequently to the SSI_{index} (Fig. 10 left). The information in the latter case is expressed exclusively in terms of normalized stiffness, and thus remains independent from the mass of the model. Both the coefficient of determination and the coefficient of variation indicate a very strong linear regression, which highlights the relative stiffness as the driving parameter that controls the level of period elongation. Considering the fact that the simplified analytical model proves highly accurate in predicting the eigenfrequency, it may be concluded that period elongation may be computed with sufficient confidence. It should be underlined however, that a proper estimation of the equivalent *G-modulus* of the soil is necessary for the calculation of the foundation-stiffness.

The experimental proof of this regression supports the case-history observations on actual bridge piers, described in [23], and provides a valuable benchmark for the assessment of real structures, as well as of further experimental data. The identified damping demonstrates an increasing trend with relative stiffness (Fig. 10 right). For the same superstructure, stiffer foundation yields lower strains and therefore mobilizes lower material damping.

The impulse intensity level is defined qualitatively, depending on the size of the spheres described in Table 1. The identified eigenfrequency is independent from the intensity level, as expected, since the intensity level is low and the response remains in the theoretical "elastic region". However, as described in Section 4.1, a drop in eigenfrequency is observed at the beginning of the oscillation, which indicates nonlinear response. This drop is quantified as a percentage of the identified eigenfrequency and is plotted as a function of the impulse intensity level (Fig. 11 left). The drop increases with increasing intensity of the impulse, indicating stronger nonlinear effects. Considering the fact that the maximum moment amplitude remains below 10% of the ultimate moment, the observation of nonlinear effects contradicts the theoretical perception of the "linear elastic range" at small strains. The *IDR* also becomes larger with increasing intensity, which leads to larger strains (Fig. 11 right). The strain dependency of the *IDR* confirms that the dominant dissipation mechanism is hysteretic and supports the conclusion that nonlinear behavior takes place even at small strains.

The identified damping plotted against the normalized frequency indicates a linear decrease (Fig. 12). The experimentally observed trend contradicts the analytical predictions that suggest larger damping values for higher oscillation frequencies, following the assumption of viscoelasticity. The *IDR* increases with increasing *PLR*, while the analytical estimations are not indicative of such a trend (Fig. 13). Higher values of frequency, as well as lower values of *PLR* are indicative of stiffer systems. Thus, both tendencies of the identified damping imply that damping decreases for stiffer systems, as a stiffer system generates lower strains and thus mobilizes less soil hysteretic action. The *PLR* does not demonstrate any sensitivity to the eigenfrequency of the system.

Higher soil density results in an increase of the system's frequency and a decrease in damping of an order of 10%. Considering the very small difference between loose and dense soil in terms of dry density, the identified effect on the modal characteristics implies that the system response is very sensitive to the soil density. It is known that soil density affects the shear strength and consequently the G-modulus, which is highlighted as the driving soil parameter for the analytical model. Both the increase in eigenfrequency and the decrease in damping reflect the increase of system-stiffness due to the "stiffening" of the soil.

Adoption of a safety factor for the bearing capacity of the soil against static vertical loads (FS_V) comprises a common engineering practice. A higher safety factor is universally considered to operate towards the safe side for static loading. In case of dynamic excitation however, the role of the FS_V is controversial. The presented results indicate an expected raise of the system-stiffness with increasing FS_V (Fig. 14 left), as the FS_V increases for deeper embedment and larger footing dimensions, both leading to a stiffer foundation. On the contrary, the SSI effects, both in terms of PLR and damping, are significantly reduced for larger values of FS_V (Fig. 14 right, Fig. 15 left). The key issue in this case is the "stiffening" of the foundation. It is shown in Fig. 10 that the SSI effects escalate with increasing relative stiffness. As a result, stiffer foundation prevents the amplification of the SSI effects. Particularly to what damping is concerned, it is mentioned that the stiffer the foundation is, the less material damping is mobilized.

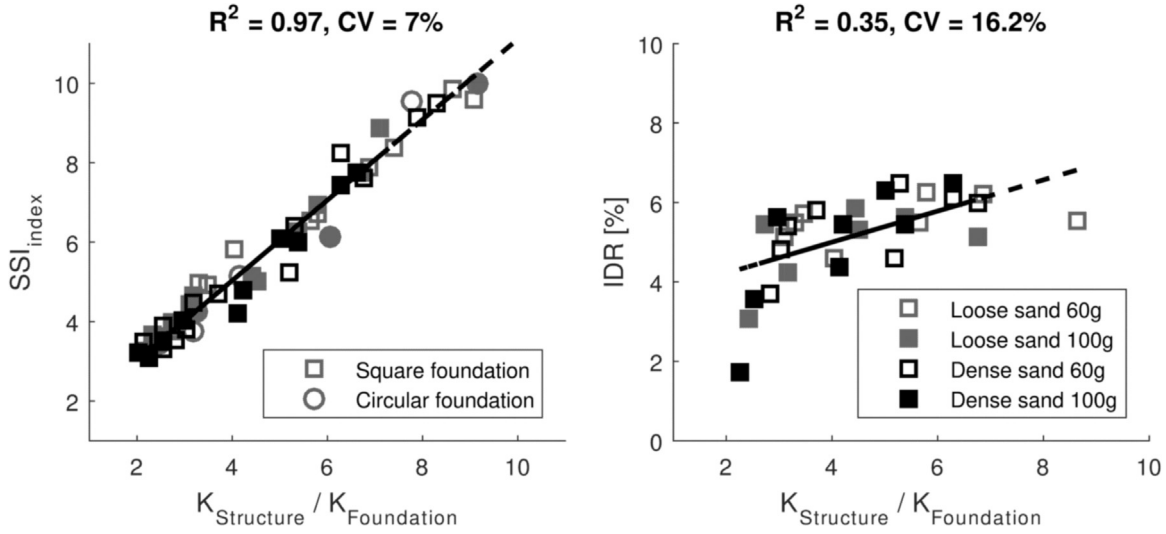

Fig. 10. Left: SSI_{index} – Relative stiffness, right: IDR– Relative stiffness.

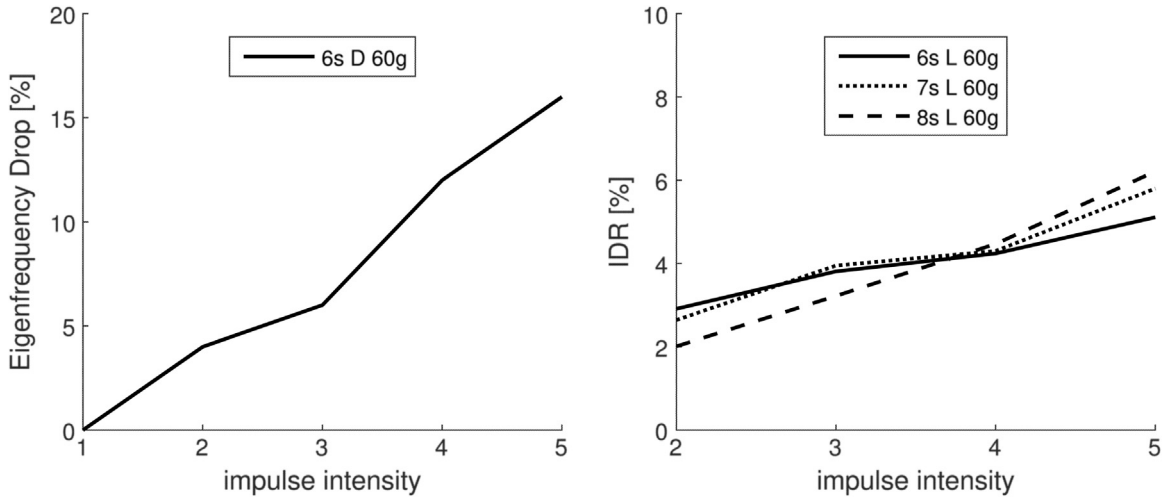

Fig. 11. Left: Impulse intensity level vs. Eigenfrequency drop right: Impulse intensity level vs. IDR.

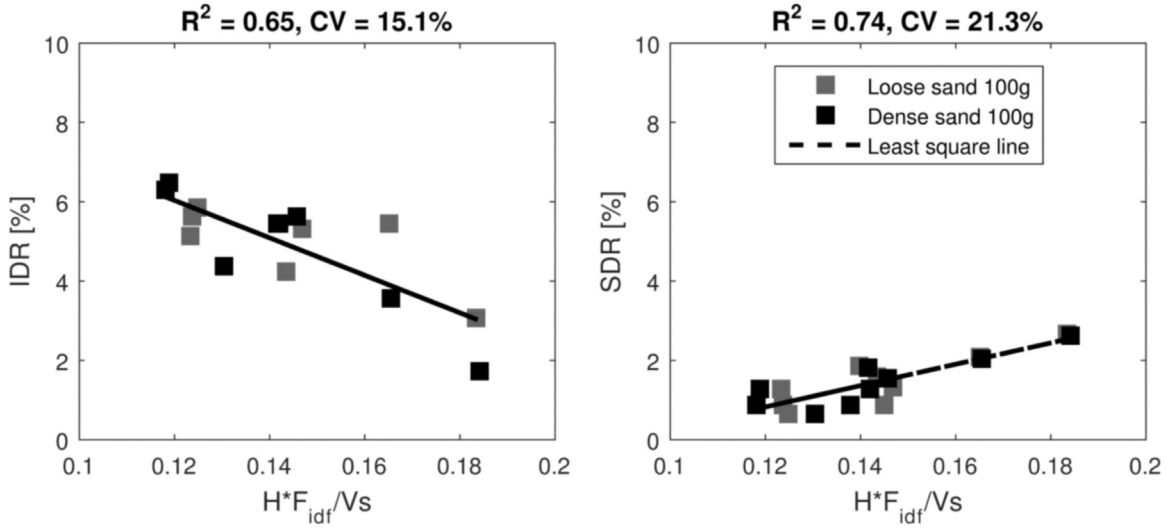

Fig. 12. Left: IDR – Normalized frequency, right: SDR – Normalized frequency.

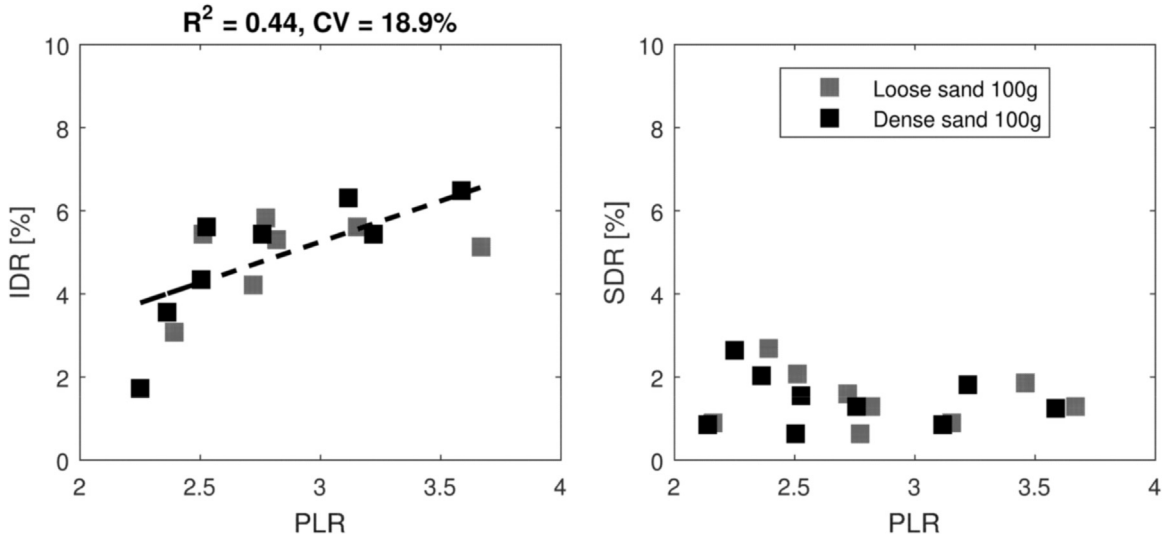

Fig. 13. Left: IDR- PLR, right: SDR-PLR.

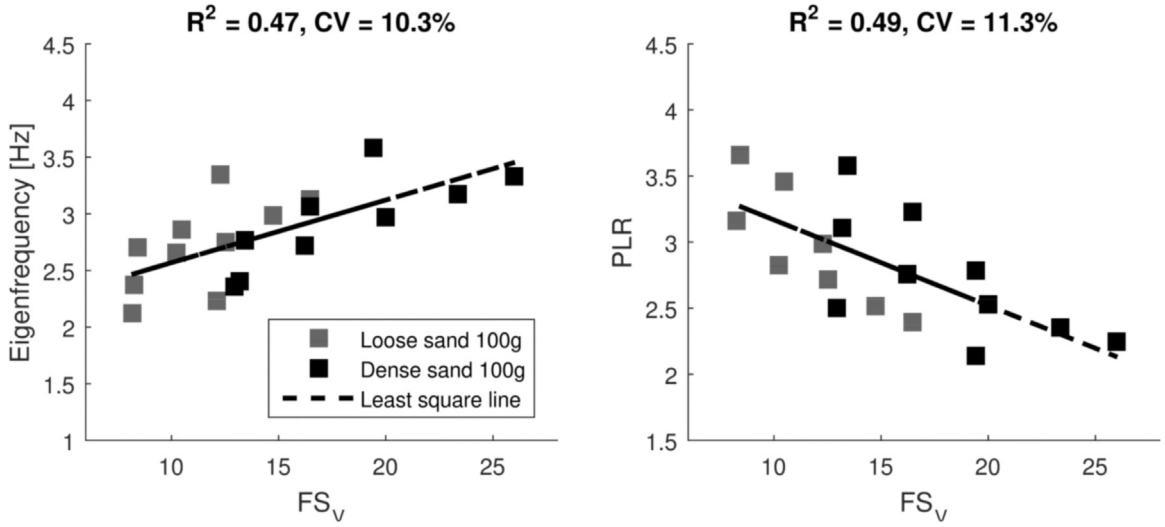

Fig. 14. Left: Eigenfrequency – FS_V, right: PLR – FS_V.

The analytically estimated *SDR* shows an opposite trend, which could foment the misleading perception that the system damping increases with increasing FS_V, and thus lead the design to the unsafe side.

The effect of the shape of the foundation is prominent in terms of eigenfrequency and *PLR*. The circular footings are less stiff than the square ones, as depicted in Fig. 16 left. Consequently, the *PLR* is larger for circular footings, since the superstructure stiffness is the same (Fig. 16 right). Regarding system damping, no clear trend can be identified, although based on the previous analysis, it would be expected that damping would be larger for circular footings, since the foundation stiffness decreases. Nevertheless, it should be considered that circular footings of diameter equal to the width of the corresponding square footings provide smaller surface in contact with the soil, and thus, less material damping is mobilized.

The effect of nonlinearities is investigated through examination of the modal characteristics of the "elastic-range" response before and after the nonlinear response of the system, triggered by higher-amplitude impulse excitation. The eigenfrequency of the system does not change remarkably. On the contrary, the *IDR* shows an average decline of 7.5%. During the nonlinear response large strains are generated and the sand-grains are locally rearranged and compacted. Consequently, the contact area between the foundation and the adjacent soil is reduced and thus, less material damping is mobilized. In terms of the eigenfrequency, the effect of the partial embedment seems to be compensated by the local compaction of the soil. In Table 5 are summarized the trends of the SSI effects observed in the experiments.

8. Conclusions

In contrast to current perception, this study argues that negligence of the SSI effect might not always lie on the safe side. The seismic demand increases for stiffer structures due to period elongation, whereas more flexible structures suffer from increasing displacement- and ductility-demand. Furthermore, the period shift could lead to resonance effects with detrimental implications. Experiments in centrifuge offer a unique opportunity to study the SSI phenomenon through parametric experimental sessions of scaled models in realistic stress and strain soil conditions. In existing literature only few well documented SSI case studies are found, while the small-scale experimental studies fail to capture realistic confining-stress conditions. Experiments in a centrifuge facility overcome this obstacle, having to face however other challenges, termed as scale effects. Most of these experiments focus on the highly nonlinear range of the response, during cyclic or earthquake loading. Before reaching the nonlinear plateau, the response is so far considered to be linear elastic and energy is assumed dissipated primarily via radiation. Nevertheless, indications of nonlinearities in small

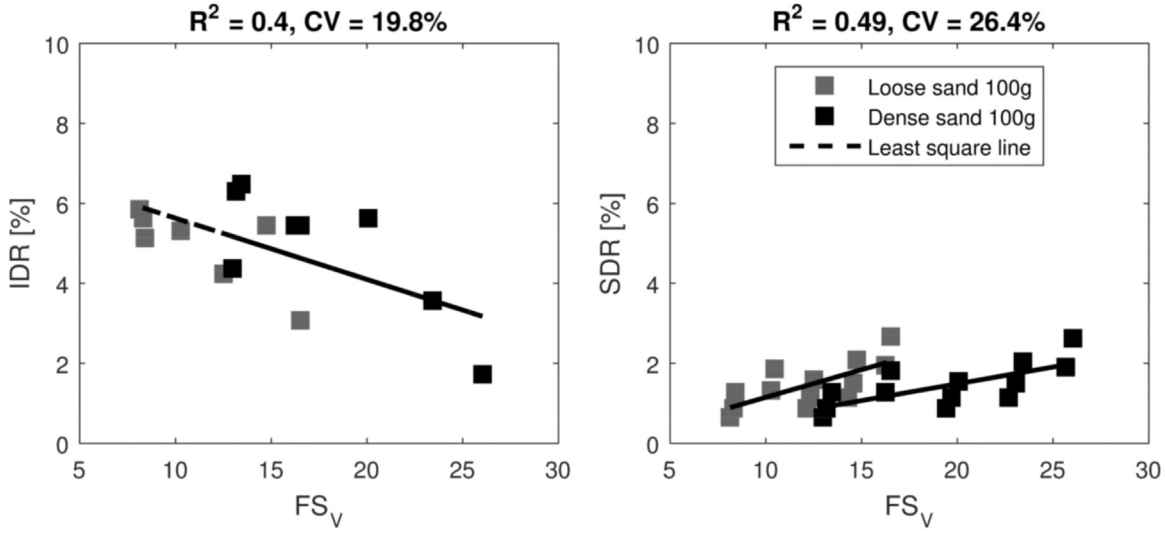

Fig. 15. Left: IDR - FS_V, Right: SDR – FS_V.

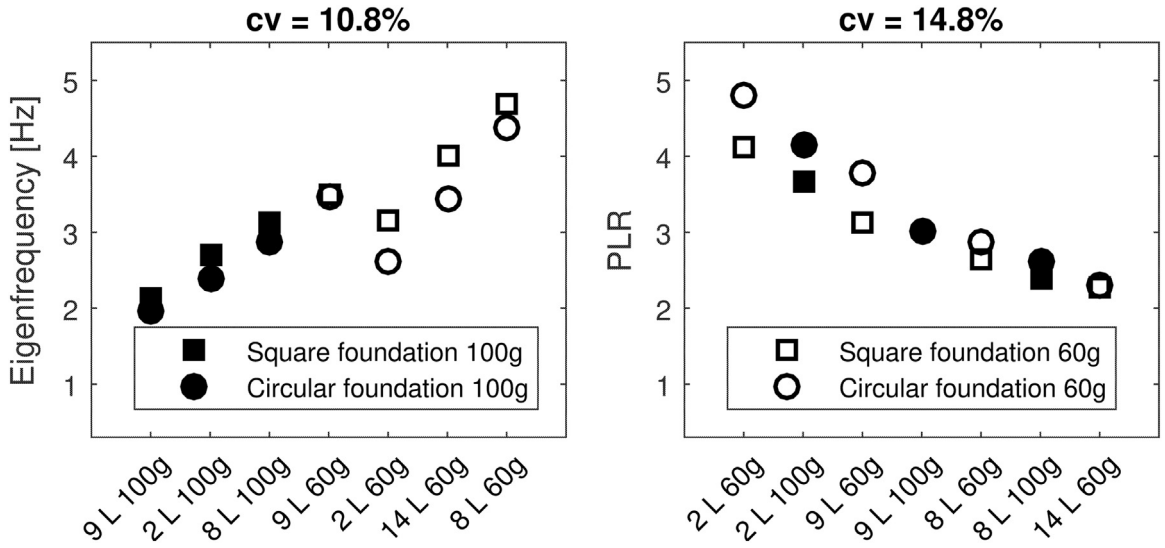

Fig. 16. Effect of the foundation shape on eigenfrequency and PLR.

Table 5
Summarize of the trends observed in the experiments.

Increasing parameter:	*D/B*	*Relative stiffness*	*Intensity level*	*Soil density*	FS_V	*Foundation shape*
Eigenfrequency	+			+	+	−
PLR		+		−	−	+
SDR		+	+	−	−	

strain-levels have already been mentioned in [40]. No experimental studies regarding this phenomenon for SSI systems came to the attention of the authors.

The most important findings of the present work may be summarized as follows:

- The simplified analytical model proves adept in estimating the eigenfrequency of the SSI system, albeit after proper calibration of the G-modulus.
- In order to ensure that the system response remains in the elastic range, the amplitude of the base moment remained below 10% of the ultimate moment during all present experiments. Nevertheless, nonlinear characteristics, such as eigenfrequency-shift and strain-dependency of damping, were identified. The observation of nonlinear effects contradicts the theoretical perception of a “linear elastic range” of the response at small strains.
- Due to nonlinear effects, the identification of the equivalent viscous damping may not be achieved through standard methods. Therefore, a modification of the Dissipated Energy method, that applies for free vibration response, is suggested and implemented.
- The eigenfrequency of the system increases with increasing foundation dimensions and soil density and is 10% higher for square foundation in comparison to circular.
- The *PLR* and the *SSI indices* in particular, indicate a strong linear dependence on the relative stiffness between the fixed-based superstructure and the foundation. Considering the fact that the simplified analytical model proves highly accurate in predicting the system's eigenfrequency, it is concluded that period elongation may be computed with sufficient accuracy in the analytical sense. It should be underlined, however, that a proper estimation of the equivalent G-modulus of the soil is necessary.
- For the same structural model, the *PLR* is inversely proportional to the foundation stiffness. Consequently, larger foundation and stiffer soil suppress the period elongation effect.
- The identified damping ratio results remarkably higher than the analytically predicted *SDR*, indicating substantial contribution of the material damping mechanism.
- Most importantly, the identified damping is not a parallel offset of the analytical predictions, as would be expected for constant material damping. Opposite tendencies between theoretical and experimentally identified damping are observed in terms of numerous parameters, exposing the insufficiency of the analytical model in capturing the actual dissipation mechanism even in the small strain range.
- The system damping is highly strain-dependent, and is thus attributed to the hysteretic action of the soil. Considering the fact that the response is limited to the “linear elastic range”, the existence of hysteretic damping contradicts the analytical perception that radiation is the dominant dissipation mechanism in the small strain range.
- A slight increase of soil dry density results in an increase of frequency and a decrease of damping in the order of 10%, implying that the system is very sensitive to the dry density of the sand and consequently to the G-modulus, which is highlighted as the driving soil parameter for the analytical model.
- The effect of the foundation shape is prominent in terms of eigenfrequency and *PLR*. The circular footings are less stiff than the square. Consequently, the *PLR* is larger for circular footings, since the superstructure stiffness remains unchanged, leading to an increase in relative stiffness. Regarding the damping of the system, no clear trend could be identified. Although the reduced foundation stiffness allows for larger strains, the reduced contact-surface with the soil decreases the mobilized damping.
- After undergoing nonlinear strains, the damping of the system in the elastic range decreases by 7.6%. This is attributed to the reduction of the contact area between foundation and soil due to local compaction. To what the system's eigenfrequency is concerned, the effect of the partial embedment seems to be compensated by local compaction of the soil and the consequent increase of its shear strength, therefore no significant differences were observed.

It need be noted that this analysis overviews a first attempt, which is subjected to a number of limitations, namely the lack of direct measurement of the structure displacements, the applied load and the soil strains. The study is limited to a simplified type of structural foundation and ideal ground conditions. Moreover, the scalability of the energy dissipation is not a straightforward issue and, thus, further research is required in order to extrapolate confidently the results to a practical

setting. That being said, this comprehensive experimental investigation offers valuable insight to the underlying mechanisms involved and motivates for further targeted research. A more extended study is to follow, addressing the aforementioned concerns.

Acknowledgement

The authors acknowledge the support of the European Research Council via the ERC Starting Grant WINDMIL (ERC-2015-StG #679843) on the topic of Smart Monitoring, Inspection and Life-Cycle Assessment of Wind Turbines. The authors are deeply indebted to Prof. Dr. Sextos Anastasios and Ph.D. candidate Faraonis Periklis for their input to the research. The authors would like to express their gratitude to Prof. Dr. Anastasopoulos Ioannis for his support, as well as to the staff of the Centrifuge facility of ETH (Dipl-Ing Herzog Ralf and Iten Markus) and to the Master students that collaborated to the research (Buss Christian, Lampach Laurent, Minu Lee and Tran Duc Thong). Prof. Chatzi would additionally like to gratefully acknowledge the support of the Albert Lück Foundation (2016-25 Professur Sustainable Construction).

References

[1] Veletsos AS, Meek JW. Dynamic behaviour of building-foundation systems. Earthq Eng Struct Dyn 1974;3:121–38.
[2] FEMA P-750. NEHRP Recommended seismic provisions for new buildings and other structures. Washington, DC: Building Seismic Safety Council; 2009.
[3] Veletsos a S, Verbic B. Vibration of viscoelastic foundations. Earthq Eng Struct Dyn 1973;2:87–102. http://dx.doi.org/10.1002/eqe.4290020108.
[4] Gazetas BG. Formulas and charts for impedances of surface and embedded foundations. J Geotech Eng 1991:117.
[5] Gazetas G. Analysis of machine foundation vibrations: state of the art. Int J Soil Dyn Earthq Eng 1983;2:2–42. http://dx.doi.org/10.1016/0261-7277(83)90025-6.
[6] Anastasopoulos I, Gazetas G, Loli M, Apostolou M, Gerolymos N. Soil failure can be used for seismic protection of structures. Bull Earthq Eng 2010;8:309–26. http://dx.doi.org/10.1007/s10518-009-9145-2.
[7] Anastasopoulos I, Kontoroupi T. Simplified approximate method for analysis of rocking systems accounting for soil inelasticity and foundation uplifting. Soil Dyn Earthq Eng 2014;56:28–43. http://dx.doi.org/10.1016/j.soildyn.2013.10.001.
[8] Kokkali P, Abdoun T, Anastasopoulos I. Centrifuge modeling of rocking foundations on improved soil. J Geotech Geoenviron Eng 2015;141:04015041. http://dx.doi.org/10.1061/(ASCE)GT.1943-5606.0001315.
[9] Mylonakis G, Gazetas G. Seismic soil-structure interaction: beneficial or detrimental? J Earthq Eng 2000;4:277–301. http://dx.doi.org/10.1080/13632460009350372.
[10] Luco JE, Mita A. Response of a circular foundation on a uniform half-space to elastic waves. Earthq Eng Struct Dyn 1987;15:105–18. http://dx.doi.org/10.1002/eqe.4290150108.
[11] Erden SM. Influence of shape and embedment on dynamic foundation response (Ph.D. dissertations). Univ. of Massachusetts at Amherst; 1974.
[12] Stokoe KH, Erden SM. Influence of base shape on dynamic response of surface foundations. Austin, Texas; 1985.
[13] Martakis P, Taeseri D, Chatzi E, Laue J. A centrifuge-based experimental and analytical study of the Soil and Structure Interaction effect. In: Proceedings of the 11th HSTAM Int Congr Mech May 27–30, Athens, Greece; 2016.
[14] Jones KC. Dynamic soil-structure-interaction analysis of structures in dense urban environments. 2013.
[15] Schofield A. Cambridge geotechnical centrifuge operations. Geotechnique 1980.
[16] Dove RC, Bennett JG. Scale modeling of reinforced concrete category i structures subjected to seismic loading. 1986.
[17] Anshuman J. Dynamic testing of structures using scale models; 2004.
[18] Laue J. Centrifuge technology. Work Const centrifuge Model two Extrem, Balkema; 2002. p. 75–105.
[19] Sextos A. State-of-the art report on the experimental and numerical studies related to soilstructure interaction for bridges subjected to seismic loading in E.U. and U.S.; 2012. p. 1–33.
[20] Ambrosini RD. Material damping vs. radiation damping in soil–structure interaction analysis. Comput Geotech 2006;33:86–92. http://dx.doi.org/10.1016/j.compgeo.2006.03.001.
[21] Meek J, Wolf JP. Material damping for lumped-parameter models of foundations. Earthq Engine Struct Dyn 1994;23:349–62.
[22] Gazetas G, Stokoe KH. Free Vib Embed Found: Theory Versus Exp 1992;117:1382–401.
[23] Chaudhary MTA, Abé M, Fujino Y. Identification of soil-structure interaction effect in base-isolated bridges from earthquake records. Soil Dyn Earthq Eng 2001;21:713–25. http://dx.doi.org/10.1016/S0267-7261(01)00042-2.
[24] Gomez HC, Ulusoy HS, Feng MQ. Variation of modal parameters of a highway bridge extracted from six earthquake records. Earthq Eng Struct Dyn 2013;42:565–79. http://dx.doi.org/10.1002/eqe.
[25] Sextos AG, Faraonis P, Zabel V, Wuttke F, Arndt T, Panetsos P. Soil – bridge system stiffness identification through field and laboratory measurements. J Bridg Eng ASCE 2016:1–13. http://dx.doi.org/10.1061/(ASCE)BE.1943-5592.0000917.
[26] Manos GC, Pitilakis K, Sextos A, Kourtides V, Soulis V, Thauampteh J. Field experiments for monitoring the dynamic soil-structure-foundation response of a bridge-pier model structure at a Test Site. J Struct Eng 2015;141:1–11. http://dx.doi.org/10.1061/(ASCE)ST.1943-541X.0001154.
[27] Manos GC, Kourtides V, Sextos A.G. Model bridge pier-foundation-soil interaction implementing in-situ/shear stack testing and numerical simulation. In: Proceedings of the 14th World Conf Earthq Eng Oct 12–17, Beijing, China; 2008.
[28] Gajan S, Kutter BL, Phalen JD, Hutchinson TC, Martin GR. Centrifuge modeling of load-deformation behavior of rocking shallow foundations. Soil Dyn Earthq Eng 2005;25:773–83. http://dx.doi.org/10.1016/j.soildyn.2004.11.019.
[29] Anastasopoulos I, Kourkoulis R, Gelagoti F, Papadopoulos E. Rocking response of SDOF systems on shallow improved sand: an experimental study. Soil Dyn Earthq Eng 2012;40:15–33. http://dx.doi.org/10.1016/j.soildyn.2012.04.006.
[30] Kokkali P, Asce SM, Abdoun T, Asce M, Anastasopoulos I. Centrifuge modeling of rocking foundations on improved soil. J Geotech Geoenviron Eng 2015;141:1–15. http://dx.doi.org/10.1061/(ASCE)GT.1943-5606.0001315.
[31] Dobry R, Gazetas G, Stokoe KH. Dynamic response of arbitrarily shaped foundations: experimental verification. J Geotech Eng 1986;112:136–54. http://dx.doi.org/10.1061/(ASCE)0733-9410(1986)112:2(136).
[32] Chatzis M, Smyth A. Robust modeling of the rocking problem. J Eng Mech 2011;138:247–62. http://dx.doi.org/10.1061/(ASCE)EM.1943-7889.0000329.
[33] Martakis P. A centrifuge-based experimental and analytical study of the Soil and Structure Interaction effect [Master Thesis]. ETH Zurich; 2016.
[34] Chen Z, Trombetta NW, Hutchinson TC, Mason HB, Bray JD, Kutter BL. Seismic system identification using centrifuge-based soil-structure interaction test data. J Earthq Eng 2013;17:469–96. http://dx.doi.org/10.1080/13632469.2012.762956.
[35] Chopra AK. Dynamics of structures. Third Edition 2003.
[36] Springman S, Laue J, Boyle R, White J, Zweidler A. The ETH Zurich geotechnical drum centrifuge. Int J Phys Model Geotech 2001;1:59–70.
[37] Wilmer Ferney, Morales Penuela, River dyke failure modeling under transient water conditions (Ph.D. dissertations), Publications of the Institute for Geotechnical Engineering, ETH Zurich, Vol. 247.
[38] Lo Presti D, Pedroni S, Crippa V. Maximum dry density of cohesionless soils by pluviation and by ASTM D 4253-83: a comparative study. Geotech Test J 1992;15:180–9.
[39] Gajan S, Kutter BL. Capacity, settlement, and energy dissipation of shallow footings subjected to rocking. J Geotech Geoenviron Eng 2008;134:1129–41. http://dx.doi.org/10.1061/(ASCE)1090-0241(2008)134:8(1129).
[40] Burland JB. Small is beautiful—the stiffness of soils at small strains. Can Geotech J 1989;26:499–516. http://dx.doi.org/10.1139/t89-064.
[41] Gajan S, Kutter BL, Thomas JM. Physical and numerical modeling of cyclic moment-rotation behavior of shallow foundations; 2004. p. 795–8.
[42] Terzaghi K, Peck PB, Mesri G. Soil mechanics in engineering practice. 3rd ed. 1996.